Solution Structure of a Polypeptide Dimer Comprising the Fourth Ca^{2+}-Binding Site of Troponin C by Nuclear Magnetic Resonance Spectroscopy†

Lewis E. Kay,*,‡ Julie D. Forman-Kay,‡ William D. McCubbin,§ and Cyril M. Kay§

Laboratory of Chemical Physics, Building 2, National Institute of Diabetes and Digestive and Kidney Diseases, National Institutes of Health, Bethesda, Maryland 20892, and Medical Research Council Group in Protein Structure and Function, Department of Biochemistry, University of Alberta, Edmonton, Alberta, Canada T6G 2H7

Received October 8, 1990; Revised Manuscript Received December 11, 1990

ABSTRACT: The structure of a 39 amino acid proteolytic fragment of rabbit skeletal troponin C containing the fourth Ca^{2+}-binding site has been determined by an approach involving nuclear magnetic resonance (NMR) spectroscopy combined with hybrid distance geometry–dynamical simulated annealing calculations. Hydrodynamic and NMR evidence establishes unambiguously that the fragment forms a stable dimer in solution in the presence of excess Ca^{2+}. The calculation of the dimeric structure is based on a total of 1056 experimental restraints comprising 422 interproton distances, 35 ϕ, 28 ψ, and 28 χ_1 torsion angle restraints within each subunit, 30 intermonomer distance restraints, and 6 Ca^{2+} restraints per subunit. A total of 48 final structures were calculated having an rms deviation about the mean atomic backbone coordinate positions of 1.0 Å for residues Asp128–Glu156. The solution structure consists of a dimer of helix–loop–helix motifs related by a 2-fold axis of symmetry. The overall architecture of the dimer is very similar to the C-terminal domain in the crystal structure of chicken skeletal troponin C.

The molecular interactions associated with muscle contraction have stimulated considerable interest from a structural perspective (Strynadka & James, 1989). Detailed hydrodynamic (Kay et al., 1987), spectroscopic (McCubbin et al., 1986; Grabarek et al., 1986; Drakenburg et al., 1987; Marsden et al., 1989; Tao et al., 1989), and X-ray crystallographic (Herzberg & James, 1985, 1988; Sundaralingam et al., 1985; Satyshur et al., 1988) studies have been performed on both the individual components of the contractile system and on their complexes. Central to the muscle contraction apparatus is troponin C (TnC)[1], a member of the troponin complex that forms part of the thin filament (Ebashi & Kodama, 1965). Binding of Ca^{2+} to TnC triggers a series of conformational changes that are propagated through the troponin complex leading eventually to muscle contraction (Huxley, 1974). In order to provide a detailed molecular framework to describe these events, X-ray crystal structure analyses have been reported for turkey skeletal muscle TnC (Herzberg & James, 1985) and chicken skeletal muscle TnC (Sundaralingham et al., 1985). Both structures reveal a dumbbell-shaped molecule with N- and C-terminal globular domains connected via a long central helix consisting of 31 residues. Each of the globular domains consists, in turn, of two helix–loop–helix motifs that form the Ca^{2+}-binding sites in the molecule. This helix–loop–helix arrangement is termed the "EF" hand. All Ca^{2+}-binding proteins for which high-resolution structures are available contain pairs of EF hands, which has lead to the hypothesis that Ca^{2+}-binding proteins have evolved through duplications of a precursor gene coding for an EF hand polypeptide (Goodman, 1980). It is of considerable interest, therefore, to initiate a detailed structural study of a single EF hand polypeptide in solution.

Recently, it has been demonstrated that two-dimensional nuclear magnetic resonance spectroscopy (NMR) can provide detailed solution structures of small proteins (Wüthrich, 1986, 1989; Clore & Gronenborn, 1987, 1989). In addition, the technique offers the potential of studying fragments of proteins that may prove difficult to crystallize. In this paper we report the solution structure of a 39 amino acid fragment of rabbit skeletal TnC containing the fourth EF hand, TH2, obtained by using 2D NMR techniques and hybrid distance geometry–dynamical simulated annealing calculations (Nilges et al, 1988). We also provide hydrodynamic and NMR evidence that indicates conclusively that the fragment exists as a dimer in solution. A comparison of the solution structure of the dimer with the crystal structure of the intact C terminus of chicken skeletal TnC is also presented.

Experimental Procedures

Purification of the TH2 Fragment from Rabbit Skeletal TnC. Digestion of TnC with thrombin was performed as described by Grabarek et al. (1981), with an incubation time of 24 h and 5 NIH units of thrombin (Sigma) used per milligram of TnC. The separation of two major peptides, TH1 (amino acid residues 1–120) and TH2 (amino acid residues 121–159), was achieved by chromatography on a Sephadex G-100 superfine column (1.5 × 120 cm) in 50 mM NH_4HCO_3 and 0.1 mM EDTA. Final purification of TH2 employed reverse-phase liquid chromatography on a SynChropak RP-P (C_{18}) 10 × 250 mm column. The initial solvent was 10%

† This work was supported by the AIDS Directed Anti-Viral Program of the Office of the Director of the National Institutes of Health (Angela M. Gronenborn, G. Marius Clore, and Ad Bax), the Medical Research Council of Canada (C.M.K.), and the Alberta Heart and Stroke Foundation (C.M.K.) L.E.K. acknowledges financial support from the Medical Research Council of Canada and the Alberta Heritage Foundation.

‡ Laboratory of Chemical Physics, NIDDKD, NIH.

§ Medical Research Council Group in Protein Structure and Function, University of Alberta.

[1] Abbreviations: CaM, calmodulin; COSY, two-dimensional correlated spectroscopy; HLH, helix–loop–helix; HOHAHA, two-dimensional homonuclear Hartman–Hahn spectroscopy; ICaBP, intestinal calcium-binding protein; MES, 2-(*N*-morpholino)ethanesulfonic acid; NOE, nuclear Overhauser effect; NOESY, two-dimensional nuclear Overhauser enhancement spectroscopy; PE-COSY, primitive exclusive two-dimensional correlated spectroscopy; Parv, parvalbumin; rms, root mean square; R_s, Stokes radius; SA, simulated annealing; TH2, thrombin fragment of TnC containing residues 121–159; TnC, troponin C.

0006-2960/91/0430-4323$02.50/0

acetonitrile/0.1% trifluoroacetic acid (TFA), and the peptide was eluted with a linear gradient to 70% acetonitrile/0.1% TFA at a flow rate of 3 mL/min, over 50 min. TH2 was found to elute near 24 min under these conditions. The material appeared as a single band on SDS–polyacrylamide (20%) gels.

Sample Preparation for Hydrodynamic Studies. Lyophilized TH2 was dissolved in a 100 mM NaCl, 25 mM 2-(*N*-morpholino)ethanesulfonic acid (MES), pH 6.0, buffer solution. One portion of this sample was then dialyzed against the original buffer solution. Another portion was dialyzed against 100 mM NaCl, 25 mM MES (pH 6.0), and 67.5 mM $CaCl_2$ to give a Ca^{2+} concentration that was in 60-fold molar excess over the peptide concentration. Both samples were dialyzed for 45 h at 4 °C. Aliquots of 220 μL of each sample were used for sedimentation equilibrium experiments, and 10-μL aliquots were used for gel-filtration experiments.

Sedimentation Equilibrium. Sedimentation equilibrium experiments were performed at 20 °C by using conventional low-speed techniques and a Beckman model E analytical ultracentrifuge equipped with Rayleigh interference optics, a titanium rotor, and 12-mm double-sector charcoal-filled Epon centerpieces. TH2 samples with and without Ca^{2+} were run for 48 h at 44 000 rpm and 34 000 rpm, respectively. Equilibrium photographs were measured manually at a magnification of 50× on a Nikon model 6 microcomparator. Molecular weight calculations were carried out with a computer program written in the APL language. Data of the form ln y vs r^2, where y is the optical density and r is the distance traveled in the centrifuge cell, were fitted to a second-degree polynomial equation by using least-squares techniques. The point-average molecular weights were calculated from the slope of this equation. A value of 0.701 was used for the partial specific volume of TH2 in the molecular weight calculations (Byers & Kay, 1982).

Gel Filtration. Gel-filtration experiments were performed at room temperature by using a TSK-G2000 SW column connected to a Varian Vista 5500 HPLC. The solvent flow rate was set at 1 mL/min, and UV absorbance was detected at 220 nm. For each TH2 sample, the solvent was identical with the dialysis buffer. The column was calibrated with respect to Stokes radius (R_s) by using cytochrome *c*, chymotrypsinogen, carbonic anhydrase, β-lactoglobulin, ovalbumin, and bovine serum albumin as standards. The void volume (V_o) and the total included volume (V_T) were measured with thyroglobulin and NaN_3, respectively. Elution volumes (V_e) of the protein standards were used to calculate the partition coefficients (σ) by the relationship

$$\sigma = (V_e - V_o)/(V_T - V_o)$$

The Stokes radii of TH2 samples were then calculated from standard curves of log R_s vs σ (Siegel & Monty, 1966). Molecular weights of TH2 samples with and without Ca^{2+} were also calculated from standard curves of log MW vs σ.

Sample Preparation for NMR Studies. Lyophilized TH2 (~4.5 mg) was dissolved in 0.5 mL of 90% H_2O/10% D_2O or 0.5 mL of 99.99% D_2O. An approximately 60-fold molar excess of $CaCl_2$ was added to the samples, which were subsequently adjusted to pH 6.0. No buffer was used.

NMR Spectroscopy. ^1H NMR spectra were recorded on a Bruker AM600 spectrometer and were processed on an ASPECT 3000 computer. All spectra were recorded in the pure phase absorption mode by using the time-proportional phase incrementation method to obtain quadrature in F_1 (Redfield & Kunz, 1975; Bodenhausen et al., 1980; Marion & Wüthrich, 1983). HOHAHA (Braunschweiler & Ernst, 1983; Davis & Bax, 1985) and NOESY (Jeener et al., 1979; Macura et al., 1981) spectra were recorded at 25 °C and 36 °C in both H_2O and D_2O. For the NOESY experiments, a mixing time of 150 ms was employed for sequential assignment and cross-peak intensity quantification of interresidue NOEs. A NOESY experiment with a mixing time of 50 ms was utilized to obtain quantitative measures of intraresidue and sequential NOE intensities involving NH, $C^\alpha H$, and $C^\beta H$ protons. HOHAHA spectra were recorded with mixing times ranging from 29 to 43 ms by using a WALTZ17 (Bax, 1989) anisotropic mixing sequence sandwiched between 1.5-ms trim pulses. In the case of NOESY and HOHAHA spectra recorded in H_2O, the water resonance was suppressed by using a semiselective jump–return read sequence (Plateau & Guéron, 1982; Bax et al., 1987). A PE-COSY spectrum (Mueller, 1987) was recorded in H_2O at 35 °C, pH 6.0, by using the method of Marion and Bax (1988a). Water supression was achieved with weak coherent presaturation, and $C^\alpha H$ resonances situated near the H_2O resonance were allowed to recover by using the SCUBA sequence (Brown et al., 1988). For NOESY and HOHAHA experiments, 1024 t_1 increments of 2K data points were collected and processed to give a resolution of 4 Hz/point in both dimensions. For PE-COSY experiments, 1024 t_1 increments of 2K data points were collected, and the FIDs were zero-filled to 1 Hz/point in the F_2 dimension. Spectra obtained with the jump–return water-suppression sequence were processed by zeroing the first point and linearly base-line correcting the free induction decay prior to Fourier transformation in the F_2 dimension and linearly base-line correcting the F_2 cross sections before Fourier transformation in F_1 (Driscoll et al., 1989). For all experiments, base-line distortion in F_2 was minimized by adjusting the receiver phase and the delay time between the final pulse and the detection period so that zero- and first-order phase corrections were −90° and 180°, respectively (Marion & Bax, 1988b). $^3J_{\alpha\beta}$ coupling constants were measured directly from the reduced multiplets in a PE-COSY spectrum recorded in D_2O by using a 35° mixing pulse. $^3J_{HN\alpha}$ coupling constants were obtained from the experimental peak-to-peak separation of each $C^\alpha H(F_1)$–$NH(F_2)$ cross peak measured in PE-COSY spectra recorded in H_2O. Because the antiphase multiplet structure of COSY peaks gives rise to an overestimation of $^3J_{HN\alpha}$ (Neuhaus et al., 1985), values measured in this way were used as upper bounds only.

Structure Calculations. The three-dimensional structures of TH2 were calculated on the basis of 874 interproton distance restraints. This comprised 194 intraresidue NOEs, 110 sequential NOEs ($|i-j| = 1$), 98 short-range NOEs ($1 < |i-j| \leq 5$), and 20 long-range NOEs ($|i-j| > 5$) per subunit and 15 intermonomer NOEs (corresponding to a total of 30 intersubunit restriants). The interresidue NOEs were classified on the basis of 150-ms spectra into strong, medium, weak, and very weak, corresponding to interproton distance restraints of 1.8–2.7, 1.8–3.3, 1.8–5.0, and 1.8–6.0 Å. Intraresidue NOE restraints were obtained from spectra recorded with mixing times of 50 ms and classified in an identical way. In addition to the interproton distance restraints, restraints from the Ca^{2+} ions to the ligands at positions 1(X), 3(Y), 5(Z), 7(−Y), and 12(−Z) of the Ca^{2+}-binding loop were included. These Ca^{2+}-binding ligand positions are found to be conserved in X-ray crystal structures of all helix–loop–helix (HLH) proteins studied to date (Strynadka & James, 1989). This nomenclature for the ligand positions is taken from the original octahedral description of the Ca^{2+} coordination (Kretsinger & Nockolds, 1973). Each of the first four positions contributes a single oxygen ligand to the coordination complex, with the

invariant Glu found in position 12 contributing both side-chain carboxyl oxygens. In the published crystal structures of TnC, the seventh position in the complex is occupied by water (Herzberg & James, 1985, 1988; Satyshur et al., 1988). This water was not included in the NMR structure calculations. Since an average Ca^{2+}–ligand distance of ~2.4 Å is obtained from X-ray crystal structure analyses of HLH proteins (Strynadka & James, 1989), the ligand Ca^{2+}–metal distances used in this study were inserted as restraints of 2.0–2.7 Å and were treated in the same fashion as the interproton distance restraints in the calculation. No restraints were used to confine the coordination geometry to pentagonal bipyramidal. Stereospecific assignments were made for as many β-methylene protons as possible. These were obtained on the basis of $^3J_{HN\alpha}$ and $^3J_{\alpha\beta}$ coupling constants and approximate distance restraints derived from intraresidue and sequential NOEs involving NH, $C^\alpha H$, and $C^\beta H$ protons, by using the conformational grid search program STEREOSEARCH (Nilges et al., 1990). In this way, 11 of the 23 nondegenerate β-methylenes were stereospecifically assigned. In addition to providing stereospecific assignments where possible, the program also provides values of the torsion angles ϕ, ψ, and χ_1 consistent with the input experimental NOE intensities and coupling constants. A total of 35 ϕ, 28 ψ and 28 χ_1 torsion angle restraints per subunit were obtained in this manner. The minimum ranges of the ϕ, ψ, and χ_1 torsion angle restraints used in these calculations were ±30°, ±50°, and ±20°, respectively (Kraulis et al., 1989).

The structures were computed from the experimental restraints by using the hybrid distance geometry–dynamical simulated annealing method of Nilges et al. (1988a) with the programs DISGEO (Havel & Wüthrich, 1984; Havel, 1986) and X-PLOR (Brünger et al., 1987; Brünger, 1988). The latter is a molecular mechanics program derived from CHARMM (Brooks et al., 1983) and includes the appropriate pseudopotentials for dynamical simulated annealing with NMR-derived restraints (Clore et al., 1985, 1986). All calculations were performed on a MicroVAX III, and the resulting structures were visualized on an Evans and Sutherland PS390 graphics system by using X-PLOR interfaced with some of the graphic features of FRODO (Jones, 1978). The hybrid protocol has been described in detail previously (Nilges et al., 1988a; Kraulis et al., 1989). Briefly, the protocol is divided into two phases. In the first phase, distance-geometry-derived structures are generated from embedding about one-third of the total number of atoms, including all backbone and most nonterminal side-chain heavy atoms from n-dimensional distance space into Cartesian coordinate space. Despite the fact that the triangle inequalities are not examined after this stage, the initial structures generated have the approximate correct fold. The remaining atoms are then added in the extended conformation, and the resultant structures subject to dynamical simulated annealing. The target function to be minimized consists of quadratic terms for bonds, angles and improper torsion angles, a quartic van der Waals repulsive potential, and square-well quadratic potential terms for interproton distance and torsion angle restraints (Nilges et al., 1988a–c). In addition, a quadratic potential is inserted to ensure that each of the monomers of the dimer is identical (see Results and Discussion). It should be stressed that *no* electrostatic, hydrogen-bonding, or 6–12 Lennard-Jones van der Waals terms are included in the calculation.

Despite the relatively small size of the TH2 fragment, the large fraction of α-helical secondary structure present in this peptide resulted in some ambiguities relating to the assignment of NOEs due to resonance overlap. In addition, the presence of equivalent monomers in the dimer led to confusion in some cases regarding the assignment of an NOE to an intra- or intermonomer restraint. These ambiguities were resolved by using an iterative strategy whereby initial structures were calculated on the basis of NOEs for which the assignment was certain (Kraulis et al., 1989; Clore et al., 1990). From the initial structures it became possible to resolve ambiguities in many of the remaining NOEs. This approach was then repeated several times. For example, an NOE between Met154 $C^\epsilon H$ and a $C^\beta H$ proton of Asp137 could not a priori be assigned as an inter- or an intramonomer NOE. After the structures were refined by using this iterative approach, the assignment became clear, since in all of the structures calculated the closet intermonomer distance between Met154 $C^\epsilon H$ and Asp137 $C^\beta H$ was 8.1 Å, while in an appreciable number of the structures the intramonomer 154 $C^\epsilon H$–137$C^\beta H$ distance was less than 5 Å. Since the steep $1/r^6$ distance dependence of the NOE precludes the observation of NOEs between protons separated by 8 Å, while NOEs between protons less than 5 Å apart are observed, it was possible to assign the Met154 $C^\epsilon H$–Asp137 $C^\beta H$ NOE to an intramonomer contact. In a similar fashion, these initial structures permitted additional stereospecific assignments to be made, since in certain cases preliminary structures had dihedral angles that fell within torsion angle ranges consistent with only one of the two potential assignments obtained with the program STEREOSEARCH (Nilges et al., 1990). Two additional stereospecific assignments involving the α-methylene protons of Gly138 and Gly144 were made in this fashion.

Results and Discussion

Prior to the 2D NMR structure determination of TH2, preliminary 1D NMR spectra of the fragment were recorded in order to ascertain qualitatively the extent of folding of TH2 in solution, both in the presence and absence of Ca^{2+}. In the absence of the metal ion, the peptide adopts a random-coil conformation, as evidenced by the lack of dispersion of resonances in the spectrum, noted particularly in the aromatic and upfield methyl-group regions and by the lack of any downfield-shifted NH and $C^\alpha H$ resonances. Upon addition of the first three or four equivalents of Ca^{2+} to the sample, very few changes were noted in the spectrum. Significant changes in the spectrum of TH2 were observed as the Ca^{2+}-to-peptide molar ratio was increased to 20:1, including the downfield migration of the NH resonance of Gly144. The appearance of a downfield-shifted NH resonance of the invariant glycine residue in position 6 of all functional Ca^{2+}-binding loops has been used as a reporter for the formation of a structured HLH fragment (Ikura et al., 1987). In the case of the TH2 fragment, the NH chemical shift of Gly144 titrates to 10.05 ppm as the Ca^{2+}-to-protein ratio is increased to ~20:1, strongly suggesting that the binding of Ca^{2+} to this fragment is in the fast-exchange limit. No significant further changes were noted in the spectrum as the concentration of metal was increased to a ratio to ~80:1. The weak binding of Ca^{2+} to TH2, as observed by NMR, is consistent with the results obtained by monitoring the ellipticity changes in the CD spectrum of TH2 at 222 nm as a function of added Ca^{2+}. From the CD data a dissociation constant for Ca^{2+} of ~1 mM can be estimated. It is interesting to note that this result is different from that reported by Shaw et al. (1990) for a 34-residue synthetic peptide representing the high-affinity Ca^{2+}-binding site III of TnC. In that case, the fragment is in a random conformation prior to the addition of the metal. However, upon titration with Ca^{2+}, the unfolded apopeptide and the structured frag-

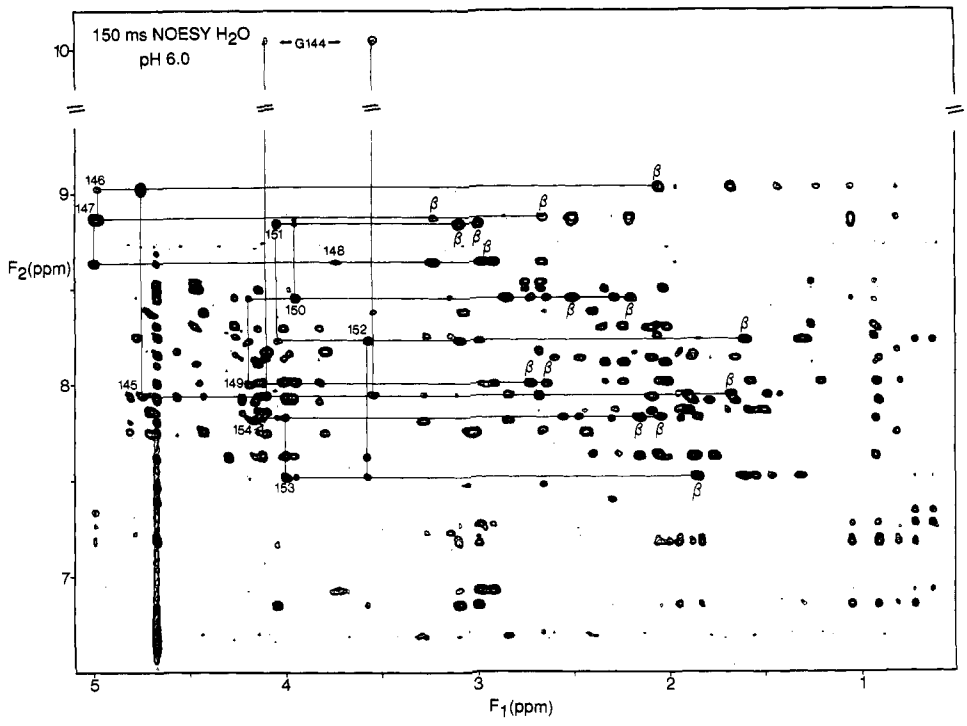

FIGURE 1: NH/aromatic (F_2 axis)–aliphatic (F_1 axis) region of the 150-ms NOESY spectrum of TH2 recorded in 90% H_2O/10% D_2O at 36 °C and pH 6.0. Selected $d_{\alpha N}(i,i+1)$ connectivities from Gly144 to Phe148 and from Asp149 to Met154 are indicated.

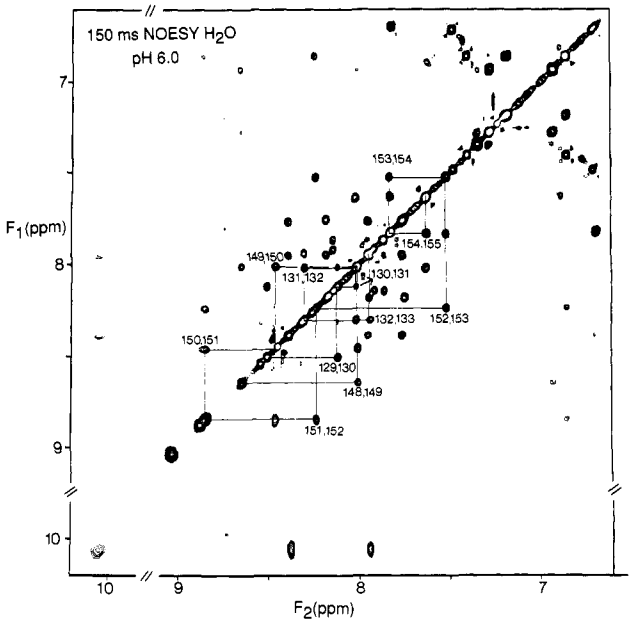

FIGURE 2: NH/aromatic (F_2 axis)–NH/aromatic (F_1 axis) region of the 150-ms NOESY spectrum of TH2 recorded in 90% H_2O/10% D_2O at 36 °C and pH 6.0. The sequence of $d_{NN}(i,i+1)$ connectivities associated with residues Glu129–Ser133 and residues Phe148–Met154 are shown.

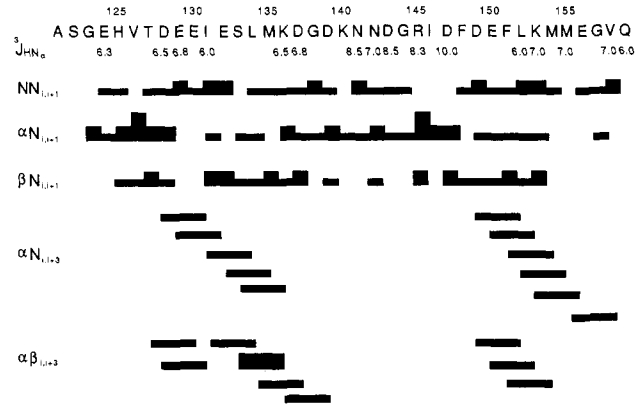

FIGURE 3: Sequence of TH2 and summary of $^3J_{HN\alpha}$ data and short-range NOEs involving NH, $C^\alpha H$, and $C^\beta H$ protons. The NOEs are classified as strong, medium, and weak as indicated by the thickness of the line. Measured $^3J_{HN\alpha}$ coupling constants are indicated below the residue's one-letter amino acid code.

ment are observed to be in slow exchange, and the titration is complete after the addition of only one equivalent of the metal, implying that the Ca^{2+} affinity of the site III fragment is considerably higher than that of TH2. This may not be surprising in lieu of published binding-constant data for proteolytic fragments of TnC that show that CB9, a 52-residue cyanogen bromide fragment containing site III, has a Ca^{2+}-binding affinity that is an order of magnitude higher than that of TH2 (Leavis et al., 1978). In order to ensure that the TH2 fragment was saturated with Ca^{2+} for our structural studies, a 60-fold excess of Ca^{2+} relative to peptide was employed in all NMR samples.

The sequential assignment of the ^1H NMR spectrum of the TH2 fragment was carried out by the conventional 2D NMR approach by using HOHAHA spectra to identify through-bond connectivities associated with intact spin systems and NOESY spectra to establish interresidue connectivities (Wüthrich, 1986; Clore & Gronenborn, 1987). In addition, PE-COSY spectra were recorded and compared with HOHAHA spectra to identify protons directly coupled in the assigned spin systems. The chemical shift assignments of the ^1H spectrum of TH2 at 36 °C are presented in Table I. Figures 1 and 2 show contour plots of the NH/aromatic–aliphatic and NH/aromatic–NH/aromatic regions, respectively, of a NOESY spectrum of TH2 recorded at 36 °C. From a qualitative interpretation of the NOESY cross-peak intensities and the $^3J_{HN\alpha}$ coupling constants derived from PE-COSY spectra, it is clear that helical segments are present in both the N- and C-terminal portions of TH2. This is indicated in Figure 3, which illustrates stretches of $d_{\alpha N}(i,i+3)$, $d_{\alpha\beta}(i,i+3)$, and $d_{NN}(i,i+1)$ connectivities conforming the

Table I: Proton Resonance Assignments of TH2 at 36 °C and pH 6.0[a]

residue	NH	$C^{\alpha}H$	$C^{\beta}H$	other
G123	8.50	3.99		
E124	8.15	4.26	1.94, 1.87	$C^{\gamma}H$ 2.17
H125	8.44	4.78	3.25, 3.13	$C^{\delta 2}H$ 7.25; $C^{\epsilon 1}H$ 8.46
V126	8.23	4.26	2.06	$C^{\gamma}H$ 0.92
T127	8.31	4.47	4.47	$C^{\gamma}H$ 1.25
D128	8.53	4.48	2.74, 2.67	
E129	8.50	4.14	2.02	$C^{\gamma}H$ 2.33
E130	8.11	4.15	2.02	$C^{\gamma}H$ 2.32, 2.23
I131	8.00	3.82	2.00	$C^{\gamma m}H$ 0.91; $C^{\gamma}H$ 1.57, 1.20; $C^{\delta}H$ 0.79
E132	8.29	4.00	2.09	$C^{\gamma}H$ 2.35, 2.23
S133	7.93	4.23	4.00, 3.95	
L134	7.91	4.16	1.87*, 1.66	$C^{\gamma}H$ 1.78; $C^{\delta}H$ 0.90
M135	8.12	4.10	2.08	$C^{\gamma}H$ 2.60, 2.46; $C^{\epsilon}H$ 1.99
K136	7.85	4.11	1.89	$C^{\gamma}H$ 1.58, 1.50; $C^{\delta}H$ 1.69; $C^{\epsilon}H$ 2.99
D137	7.93	4.56	2.67	
G138	8.16	4.10, 3.79		
D139	7.74	4.71	3.02*, 2.43	
K140	7.86	4.15	1.94, 1.90	$C^{\gamma}H$ 1.59, 1.51; $C^{\delta}H$ 1.69; $C^{\epsilon}H$ 3.03
N141	7.94	4.80	3.27, 2.84*	$N^{\delta}H_2$ 7.82, 6.70
N142	7.75	4.43	3.05, 2.65	$N^{\delta}H_2$ 7.48, 6.71
D143	8.38	4.71	3.06, 2.40*	
G144	10.05	4.10, 3.53		
R145	7.94	4.75	1.67	$C^{\gamma}H$ 1.48, 1.41; $C^{\delta}H$ 3.10
I146	9.02	4.98	2.05	$C^{\gamma m}H$ 1.05; $C^{\gamma}H$ 1.42, 1.23; $C^{\delta}H$ 0.81
D147	8.86	4.98	3.22, 2.66*	
F148	8.63	3.73	2.98, 2.91*	$C^{\delta}H$ 6.94; $C^{\epsilon}H$ 7.28; $C^{\zeta}H$ 7.35
D149	7.99	4.19	2.71*, 2.64	
E150	8.45	3.96	2.50, 2.22*	$C^{\gamma}H$ 2.85, 2.28
F151	8.83	4.04	3.09*, 2.99	$C^{\delta}H$ 6.85; $C^{\epsilon}H$ 7.18; $C^{\zeta}H$ 7.19
L152	8.22	3.57	1.60	$C^{\gamma}H$ 1.30; $C^{\delta}H$ 0.72, 0.63
K153	7.51	4.00	1.85	$C^{\gamma}H$ 1.54, 1.46; $C^{\delta}H$ 1.64; $C^{\epsilon}H$ 2.95
M154	7.82	4.11	2.15*, 2.04	$C^{\gamma}H$ 2.55, 2.47; $C^{\epsilon}H$ 1.96
M155	7.62	4.11	2.05	$C^{\gamma}H$ 2.39, 2.25; $C^{\epsilon}H$ 1.86
E156	7.62	4.29	1.87, 1.76*	$C^{\gamma}H$ 2.00
G157	8.01	4.00, 3.95		
V158	7.62	4.15	2.15	$C^{\gamma}H$ 0.92
Q159	7.81	4.16	1.93	$C^{\gamma}H$ 2.29; $N^{\epsilon}H_2$ 7.40, 6.85

[a] Chemical shifts are reported with respect to sodium 4,4-dimethyl-4-silapentane-1-sulfonate. The C^{β} methylene protons that have been stereospecifically assigned are indicated by the asterisk next to the $H^{\beta 3}$ proton.

Table II: Gel-Filtration Stokes Radius and Molecular Weight Data for TH2

Ca^{2+} state[a]	stokes radius	MW
$-Ca^{2+}$	21.3	22 700[b]
$+Ca^{2+}$	14.9[c]	10 100

[a] The minus sign refers to the absence of Ca^{2+}; the plus sign refers to the presence of 60-fold molar excess Ca^{2+} over peptide. [b] This value for the molecular weight is unrealistic, since the molecule is totally flexible and unstructured in the absence of Ca^{2+}. Under these conditions, TH2 will exhibit an abnormally high value for the Stokes radius. [c] A calculation assuming a spherical TH2 dimer particle (M_r = 8800 g/mol) yields a Stokes radius of 13.5 Å, in reasonable agreement with that measured experimentally.

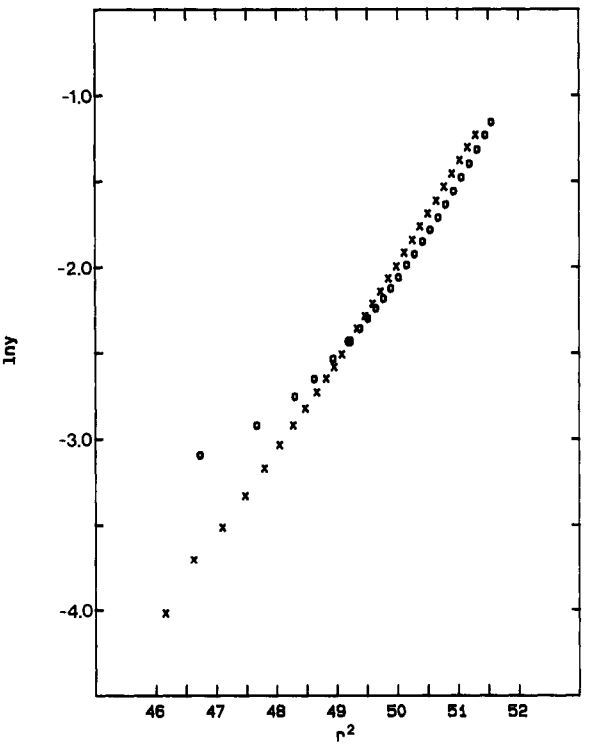

FIGURE 4: Plot of the natural logarithm of the optical activity (y) as a function of distance moved in the centrifuge cell (r). Data were recorded for TH2 in the presence (o) and absence (x) of Ca^{2+} at 20 °C, 100 mM NaCl, and 25mM MES, pH 6.0. A 60-fold molar excess of Ca^{2+} was employed in the $+Ca^{2+}$ case to parallel the concentration ratios used for NMR.

presence of helical secondary structure extending from approximately Thr127 to Asp137 and from Phe148 to Glu156. The ends of the helices cannot be determined exactly from a qualitative analysis of this sort and can only be defined more precisely from a complete structure determination.

Upon completion of the assignment of the ^1H NMR spectrum of TH2 and the preliminary secondary structure analysis, short- and long-range NOEs were assigned. During this assignment process, intense NOEs were observed between $C^{\alpha}H$ of Arg145 and $C^{\alpha}H$ of Asp147 as well as $C^{\beta}H$ of Arg145 and $C^{\alpha}H$ of Asp147. These NOEs are inconsistent with the stretch of intense sequential $d_{\alpha N}$ connectivities observed in this region and can only be explained in terms of a dimer structure. Moreover, initial structures calculated by using the hybrid distance geometry–simulated annealing approach described above only on the basis of NOEs that could be assigned to specific pairs of protons with complete confidence produced structures displaying a large number of violations of the distance restraints. In addition to the intense NOEs between $C^{\alpha}H/C^{\beta}H$ of Arg145 and $C^{\alpha}H$ of Asp147, NOEs involving the aromatic protons of Phe151 and Phe148 and $C^{\delta}H$ and $C^{\gamma m}H$ of residues Leu134 and Ile131, as well as NOEs between the $C^{\epsilon}H$ of Met154 and Met155 and $C^{\delta}H$ of residues Ile131 and Leu134, were observed that could not be explained in terms of a monomer model. At least 15 NOEs of this type were observed. The pattern of NOE discrepancies in these initial structures was suggestive of the formation of a dimer with the N terminus of one of the monomers in close contact with the C-terminal domain of the second monomer and vice versa. This would require that the monomers be oriented antiparallel to each other. Only a single set of resonances was observed in all the NMR spectra of TH2, consistent with the formation of a dimer with monomer components related by a 2-fold axis of symmetry.

Further proof for the existence of a Ca^{2+}-induced dimer was obtained by a study of the hydrodynamic properties of TH2 in the presence and absence of Ca^{2+}. Table II shows the apparent Stokes radius and molecular weight of TH2 measured with and without Ca^{2+}. In the presence of metal, the data are consistent with the formation of a dimer since the molecular weight of an individual monomer is 4400 Da. Moreover, the measured Stokes radius of 14.9 Å is in good agreement with the predicted value of 13.5 Å, assuming the formation of a spherical dimer particle. Figure 4 shows sedimentation

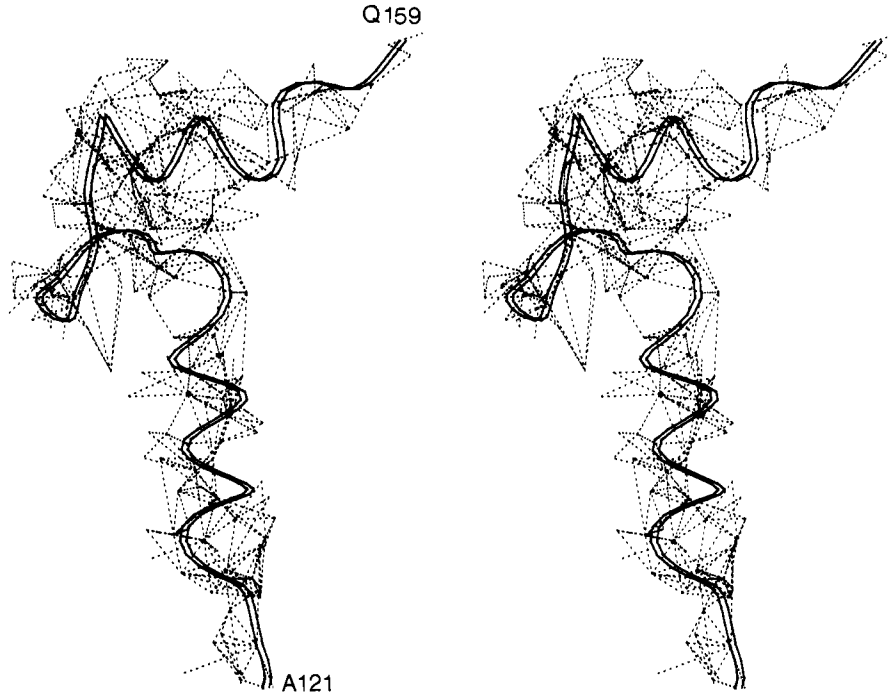

FIGURE 5: Intramonomer experimental interproton distance restraints superimposed on a smoothed backbone ribbon drawing of one monomer unit of the restrained minimized mean structure, $\overline{SA}_r$, of TH2 from Ala121 to Gln159. There are 422 NOEs indicated in the figure.

equilibrium results for the TH2 fragment in the presence and absence of Ca^{2+}. The deviation from linearity observed in the trace with Ca^{2+} indicates that, unlike the metal-free state, the monomer is not the only species in solution. At the bottom of the cell (r^2 = 51.6), a point-average molecular weight of 8865 Da is obtained, consistent with the formation of dimers at a protein concentration on the order of 3 mg/mL. This concentration is about a factor of 3 lower than in the samples used in the recording of NMR spectra. It is noteworthy that Shaw et al. (1990) independently, using 2D NOE methods on a 34-residue synthetic peptide representing the high-affinity site III of TnC, have proposed that a symmetric two-site dimer similar in tertiary structure to the C-terminal domain of TnC forms from the assembly of two site III peptides in the Ca^{2+}-bound form.

Once the existence of the dimer was established, NOEs were classified as arising from intra- or intermonomer interactions. This classification can, in general, be an extremely difficult problem whose resolution often requires isotopic labeling (Weiss, 1990; Arrowsmith et al., 1990). In this case, the situation was simplified considerably by the fact that most of the inconsistent NOEs involved contacts between residues at the N terminus of the fragment with those at the C terminus and vice versa. Because of the steep $1/r^6$ distance dependence of the NOE, these interactions must arise from protons separated by no more than approximately 6 Å in the three-dimensional structure (Clore et al., 1990). In order for the structure of the HLH fragment in solution to resemble the known structure in the intact TnC molecule, these restraints would have to be intermonomer. Certain restraints could not be assigned as intra- or intermonomer on the basis of this assumption and were therefore left out of the calculation until the structure was sufficiently refined to allow the possibilities to be distinguished. This approach for separating intra- from intermolecular contacts relies to some extent, therefore, on a qualitative appreciation of the overall fold of the protein.

A total of 48 final simulated annealing (SA) structures were calculated with residues Asp128–Glu156 having a backbone atomic rms deviation of 1.0 ± 0.2 Å about the mean. The N- and C-terminal residues, from Ala121 to Thr127 and Gly157 to Gln159, were not as well-defined due to the small number of NOEs observed, limiting the number of distance restraints for these residues. In the case of the final 48 SA structures, the NMR restraints are all satisfied, with no deviations of interproton distance or torsion angle restraints greater than 0.3 Å or 3°, respectively. In addition, deviations from ideal covalent geometry are small. The Lennard-Jones energy, calculated for the final structures, is large and negative, −198 ± 20 kcal/mol, indicating that there are no bad nonbonded contacts. Structural statistics are presented in Table III.

Figure 5 shows a stereoview of the experimental intramonomer NOE distance restraints superimposed on a smoothed ribbon backbone drawing of the restrained energy-minimized average of the 48 SA structures of TH2. For clarity, only one monomer is displayed in the figure. In total, there are 422 NOEs represented in this figure arising from intraresidue, sequential, short-range, and long-range contacts. On average, 11.4 interproton distance restraints per residue were obtained, excluding Ala121 and Ser122 since no NOEs were observed involving these residues. The average number of restraints per residue is somewhat misleading since, as the figure indicates, there is not a uniform distribution of restraints throughout the molecule. Only 16 of the 39 residues show long-range or dimer contacts. Over 70% of these contacts involve just 7 residues: Ile131, Leu134, Met135, Gly138, Asp139, Ile146, and Phe151. The presence of a small number of long-range NOEs involving only a few of the residues can be understood by considering the overall fold of the fragment. This is illustrated in Figure 6, which shows a stereoview of the superposition of the backbone positions of a set of 20 arbitrarily chosen final SA structures of TH2. Each of the monomers consists of two helices separated by a loop region that forms the Ca^{2+}-binding site. From the orientation shown in the diagram, it is clear that the two intramonomer helices are at an angle of ~90°, while the N-terminal helix of one monomer and the C-terminal helix of the second monomer are at an angle of ~120°. This arrangement minimizes both the number of possible contacts and the number of residues in-

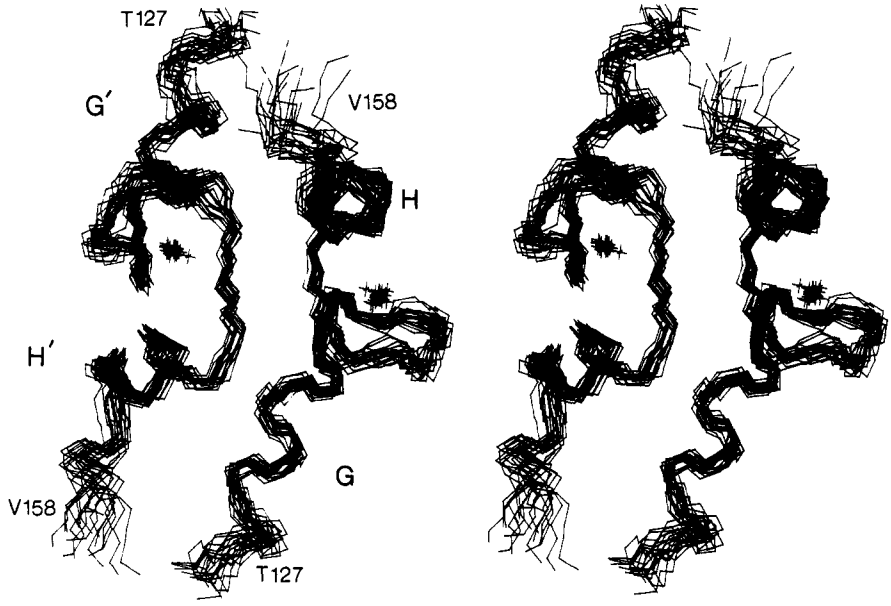

FIGURE 6: Stereoview showing the best-fit superpositions of the backbone (N, C^{α}, C) atoms of a set of 20 arbitrarily chosen final structures of TH2 from Thr127 to Val158. The view shown is looking down helix H.

volved in contacts relative to the case of two helices oriented in a more parallel fashion. Additionally, the small number of long-range and intermonomer NOEs may reflect the presence of mobility at the dimer interface.

The overall fold of the backbone involving residues Asp128–Glu156 in TH2 is quite well-defined, with the positions of the side chains on average considerably less restrained. The rms distribution of the atomic positions and torsion angles for the calculated SA structures, as well as the surface accessibility, are shown in Figure 7 as a function of residue number. Only side chains of residues Met135, Asp139, Ile146, Phe151, Leu152, and Met154 have rms deviations of less than 1 Å about the mean. On average, side chains of these residues exhibit a surface accessibility in the restrained minimized mean structure, $\overline{SA}_r$, of only 23% relative to the accessible surface area of the corresponding residue in a tripeptide Gly-X-Gly fragment (Chothia, 1976). Of the remaining side chains, nine have degenerate or near degenerate β-methylene proton chemical shifts (Glu129, Glu130, Glu132, Lys136, Asp137, Arg145, Lys153, Met155, and Gln159) and have an average fractional surface accessibility greater than 55%. Other than the residues immediately adjacent to the ends of the fragment, the portion of the loop region extending from Lys140 to Gly144 is the least well-defined part of the structure, judged by the rms difference of the positions of the backbone atoms as well as the rms deviations of the ϕ and ψ torsion angles.

With the three-dimensional structure of TH2 in hand, it is now possible to refine the description of the secondary structure of the fragment based on NOE connectivities, which was indicated previously. In the description that follows, in keeping with the nomenclature of domain IV of intact TnC (Strynadka & James, 1989), we shall refer to the N- and C-terminal helices of one of the monomers as helices G and H, respectively, and the helices associated with the other monomer will be called G′ and H′. On the basis of the hydrogen-bonding network present, as well as on $^3J_{HN\alpha}$ values, helix G extends from Thr127 to Asp137. A hydrogen bond is considered to be present if the distance between the acceptor and the donor heavy atoms is less than 3.4 Å, the angle made by the acceptor, hydrogen, and donor atoms is greater than 110°, and if these criteria are met by a substantial number of individual structures. The data suggest that two 1–4 hydrogen bonds involving Thr127–Glu130 and Asp128–Ile131 are present at the beginning of the helix, followed by the more regular 1–5 hydrogen-bonding pattern. The C-terminal end appears to tighten with several bifurcated 1–4 and 1–5 hydrogen bonds. Helix H is less regular than G, and while the start and end points are somewhat ambiguous, this helix appears to include residues Asp149–Met154. The hydrogen-bonding network appears to consist primarily of 1–4 interactions, although a 1–5 hydrogen bond between Leu152 and Glu156 is present in the majority of the structures.

A small region of β-strand is formed by residues Arg145–Asp147. An antiparallel β-sheet between the two symmetrically positioned strands forms the dimer interface, with strong intermonomer NOE contacts observed between the $C^{\alpha}H$ of Arg145 and the $C^{\alpha}H$ of Asp147 across the dimer interface. As will be described in more detail later, the side chain of Ile146 plays a very important role in stabilizing the fragment. Twenty-five restraints between Ile146 and residues located at least four residues away in the sequence were obtained, establishing this small stretch as the best defined region in the structure. Thus, the average rms backbone deviation for residues Arg145–Asp147 is 0.7 Å, compared with 1.1 Å for the helical regions.

The calcium-binding sites of the HLH proteins involve a segment of polypeptide chain with 12 contiguous residues, termed the Ca^{2+}-binding loop. The loop region extends from Asp139 to the beginning of helix H, including the small β-strand, and provides the ligands for Ca^{2+} coordination. X-ray crystal structures of TnC indicate that residues Asp139, Asn141, and Asp143 chelate Ca^{2+} by providing one oxygen from side-chain carboxyl groups. In addition, residue Glu150 donates both carboxyl oxygens, with additional ligands provided by the backbone oxygen of Arg145 and a water molecule (Herzberg & James, 1988; Satyshur et al., 1988). As indicated previously, associated with the formation of the helix–loop–helix structure is the downfield shift of the NH resonance of Gly144. The majority of the calculated structures indicate a hydrogen bond between the NH of Gly144 and one of the two δ oxygens from the side chain of Asp139. The downfield migration of the NH group observed during the course of the Ca^{2+} titrations mentioned previously may be associated with the formation of this hydrogen bond. The contribution of ring

Table III: Structural Statistics and Atomic rms Differences[a]

	⟨SA⟩	$\overline{SA_r}$
Structural Statistics		
RMS deviations from exptl distance restraints and Ca^{2+} restraints (Å)[b]		
all (886)	0.020 ± 0.002	0.028
intramonomer		
intraresidue (388)	0.016 ± 0.003	0.019
sequential ($\|i-j\| = 1$) (220)	0.024 ± 0.005	0.024
interresidue short range ($1 < \|i-j\| \leq 5$) (196)	0.020 ± 0.006	0.032
interresidue long range ($\|i-j\| > 5$) (40) with 12 Ca^{2+} restraints (52)	0.015 ± 0.007	0.020
intermonomer (30)	0.024 ± 0.010	0.062
RMS deviations from exptl dihedral restraints (deg) (182)[b]	0.080 ± 0.060	0.062
F_{NOE} (kcal/mol)[c]	4.7 ± 1.5	10.6
F_{tor} (kcal/mol)[c]	0.20 ± 0.2	0.41
F_{sym} (kcal/mol)[c]	0.57 ± 0.0	0.55
F_{repel} (kcal/mol)[c]	8.6 ± 3.2	17.0
E_{L-J} (kcal/mol)[c]	−198 ± 20	−171
Deviations from idealized geometry[d]		
bonds (Å) (1182)	0.003 ± 0.0	0.003
angles (deg) (2128)	1.72 ± 0.01	1.73
impropers (deg) (432)	0.44 ± 0.01	0.48
	backbone atoms	**all atoms**
Atomic rms Differences (Å) for Residues Asp128–Glu156		
dimer		
⟨SA⟩ vs $\overline{SA}$	1.04 ± 0.24	1.57 ± 0.20
$\overline{SA_r}$ vs $\overline{SA}$	0.30	0.73
⟨SA⟩ vs $\overline{SA_r}$	1.08 ± 0.25	1.74 ± 0.19
monomer		
$\langle SA_a \rangle$ vs $\overline{SA_a}$	0.85 ± 0.20	1.44 ± 0.16

[a] The notation of the structures is as follows: ⟨SA⟩ are the 48 final dynamical simulated annealing structures; $\overline{SA}$ is the mean structure obtained by averaging the coordinates of all 48 individual structures best fitted to each other from Asp128 to Glu156; $\overline{SA_r}$ is the restrained minimized average structure obtained from the restrained minimization of $\overline{SA}$; $\langle SA_a \rangle$ are the coordinates of the SA structures for only one subunit of the dimer; $\overline{SA_a}$ is the mean structure for a single subunit obtained by averaging the coordinates of one subunit for all 48 structures best fitted to residues Asp128 through Glu156 of a single subunit. [b] None of the structures exhibited violations greater than 0.3 Å or dihedral angle violations greater than 3°. The number of restraints for the complete dimer are indicated in parentheses. [c] The values of the square-well NOE and torsion angle potentials [cf. eq. 2 and 3 in Clore et al. (1986)] are calculated with force constants of 50 kcal mol^{-1} $Å^{-2}$ and 200 kcal mol^{-1} rad^{-2}, respectively. E_{sym} is an effective harmonic potential used to maintain symmetry between the two subunits (Brünger, 1986) with a force constant set to 300 kcal mol^{-1} $Å^{-2}$ used throughout the structure calculations (Clore et al., 1990). The value of the quartic van der Waals repulsion term [cf. eq 5 in Nilges et al. (1988)] is calculated with a force constant of 4 kcal mol^{-1} $Å^{-4}$ with the hard-sphere van der Waals radii set to 0.8 times the standard values used in the CHARMM (Brooks et al., 1983) emperical energy function. E_{L-J} is the Lennard-Jones van der Waals energy calculated with the CHARMM empirical energy function. It is not included in the simulated annealing structure calculations. [d] The number of bonds, angles, and improper torsion angles are indicated in parenthesis. The latter relate to planarity and chirality restraints.

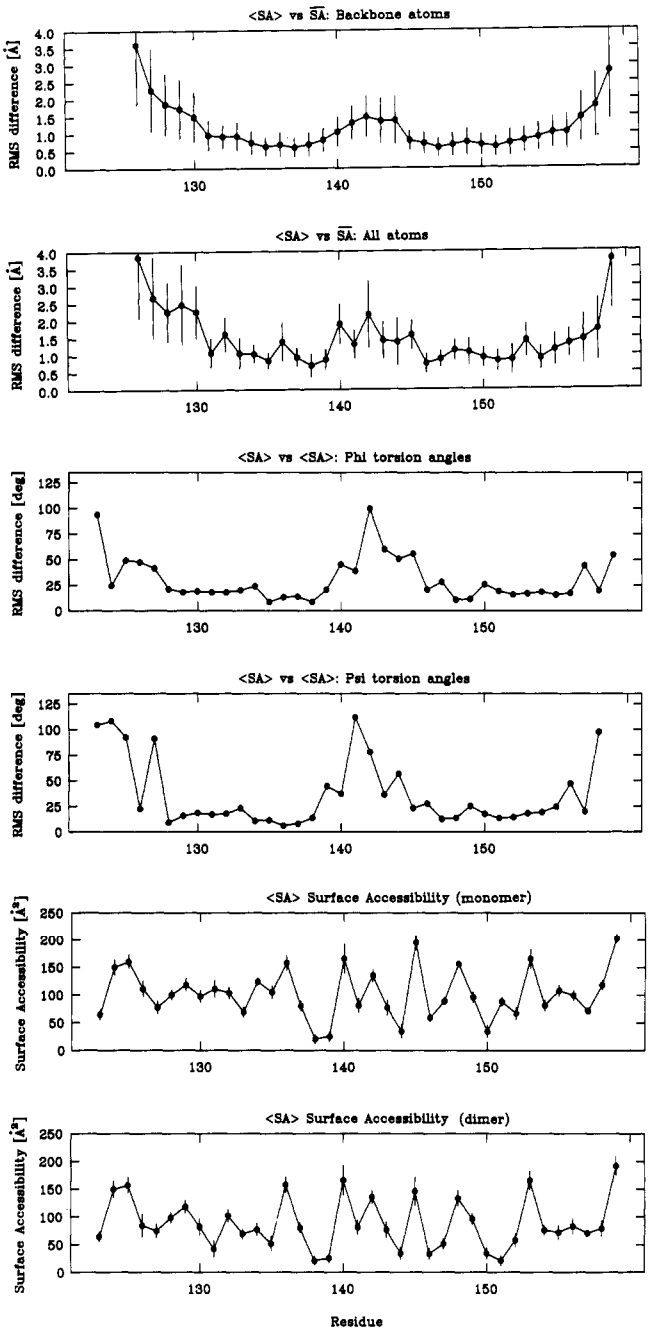

FIGURE 7: Atomic rms distribution of the final 48 individual SA structures about the mean structure, $\overline{SA}$, for backbone (N, C^{α}, C, O) atoms and all atoms and the pairwise angular rms deviations for ϕ and ψ torsion angles as a function of residue, together with the mean surface accessibility of each residue. Mean values are represented as solid circles and the error bars indicate the standard deviations in these values.

currents to the chemical shift of the NH proton of Gly144 is expected to be small since the distance between Gly144 NH and the closest aromatic residue in the structure is in excess of 11 Å. Upon metal binding, the surface accessibility of the coordinating residues decreases significantly relative to what is expected for unligated charged amino acids such as Asp and Glu. The average fractional surface accessibility of these residues in the dimer relative to the same residues in a Gly–X–Gly sequence is 0.36. In contrast, the remaining charged residues in the protein show a much higher average fractional surface accessibility of 0.66. Despite the fact that the Ca^{2+} coordination stabilizes the loop structure, the overall definition of the structure in the region from Lys140 to Gly144 is poorer than in the helical regions. For example, the rms backbone deviation about the mean is approximately 0.6 Å higher for these residues than for residues in helices G and H. This is a reflection of the small number of restraints in this region since only two short-range and one long-range NOE were observed. Additionally, values for both $^3J_{\alpha\beta 1}$ and $^3J_{\alpha\beta 2}$ of approximately 6–7 Hz were measured for Asn142, indicative of multiple side-chain conformations.

The aromatic side chains of Phe148 and Phe151, as well as the side chains of Ile131 and Leu134, form the nucleus of the hydrophobic core in TH2. These residues display numerous contacts to each other as well as to other residues.

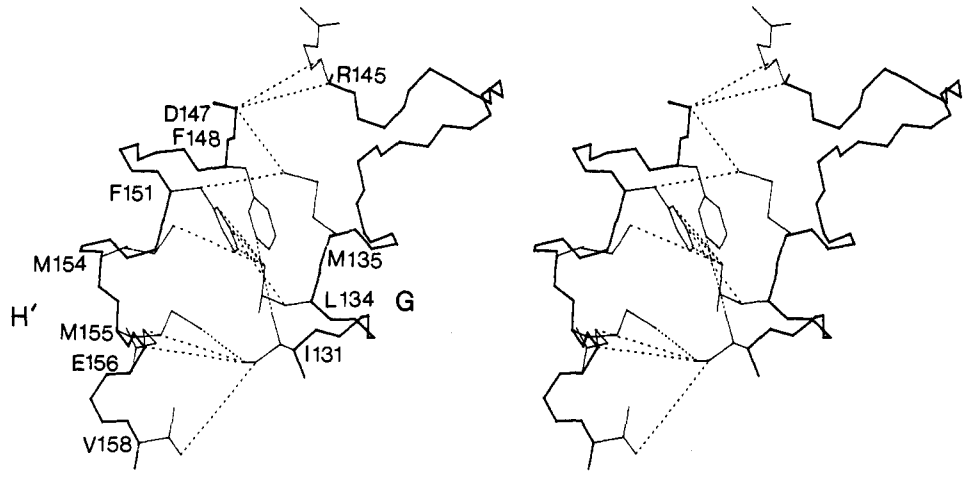

FIGURE 8: Stereoview of the restrained minimized mean structure, $\overline{SA}_r$, of TH2 looking down the antiparallel β-sheet consisting of two β-strands extending from Arg145 to Asp147. Helix G and helix H' (corresponding to helix F in the C-terminal domain of intact TnC) are shown, and the dimer contacts are indicated by the dotted lines.

Many of these additional contacts involve the $C^{\epsilon}H$ groups of the methionine residues. For example, intermonomer contacts are observed between $C^{\epsilon}H$ of Met135 and the side chain of Phe151 and between $C^{\epsilon}H$ of Met154 and $C^{\delta}H$ of Leu134 and $C^{\epsilon}H$ of Met155 and $C^{\delta}H$ of Ile131. Interestingly, in the intact rabbit skeletal TnC molecule, the interface between helices E and H consists of a set of hydrophobic interactions that involve Phe99 and Phe151, as well as Phe99 and Phe148. The aromatic residues Phe99 and Phe151 or homologous residues are found to pack against one another in the same manner in X-ray structures of troponin C(TnC) (Herzberg & James, 1988; Satyshur et al., 1988), calmodulin (CaM) (Babu et al., 1988), parvalbumin (Parv) (Kretsinger & Nockolds, 1973; Moews & Kretsinger, 1975; Swain, 1988), and intestinal calcium-binding protein (ICaBP) (Szebenyi & Moffat, 1986). In CaM, TnC, and ICaBP, Phe148 also stacks against Phe99 and Phe151. In the TH2 dimer, the conserved residue Phe99 from helix E is replaced by Met135, which as discussed above, shows a strong NOE to Phe151. The "substitution" of methionine for phenylalanine surprisingly does not affect the relative orientation of the remaining phenylalanine residues, Phe148 and Phe151. The angle between these phenyl groups in TH2 is 23 ± 19°, which is very similar to values of 21° and 27° found in the X-ray structures of TnC (Herzberg & James, 1988) and calmodulin (Babu et al., 1988). (Of the 48 final SA structures, 5 had the phenyl groups positioned such that the angle between them was more than twice the standard deviation from the mean. The average angle between the phenyl groups in the remaining structures is 18 ± 7°.) Ile146 also makes important intramonomer contacts that help to stabilize the loop region. These include interactions involving the side chains of Met135, Asp139, Phe151, and Met154, as well as contacts to the backbone protons of Gly138 and Asp139. Figure 8 illustrates the dimer contacts between helix G and helix H', corresponding to helix F in the intact structure. Table IV compares the hydrophobic contacts common to all Ca^{2+}-binding domans, based on an analysis of the crystal structures of TnC, CaM, Parv, and ICaBP, with the contacts observed in the NMR structure of TH2.

The intermonomer hydrophobic contacts described above clearly play an important role in stabilizing the structure of the dimer. Further insight into which residues are crucial for dimer formation can be obtained by examining the change in solvent accessibility as a function of residue between the monomer and dimer structures. Residues Ile131, Leu134, Met135, Arg145, Ile146, Asp147, and Phe151 show solvent accessibilities that have decreased by 39%, 28%, 29%, 22%, 15%, 25%, and 32%, respectively, relative to an isolated monomer having the same structure as in the dimer. Other residues in the fragment experience much smaller changes. Overall, a decrease in surface area of ~550 Å^2/monomer, or roughly 15% of the subunit surface, is noted upon dimer formation. This corresponds to a decrease in solvation energy of 5.5 kcal/mol upon dimer formation from the monomer structure, calculated by the method of Eisenberg and McLachlan (1985). Values for changes in surface accessibility range from 9% of the subunit surface in superoxide dismutase to 40% of the subunit surface in catalase (Janin et al., 1988) upon oligomerization from the monomer.

Table IV: Comparison between Hydrophobic Contacts Common to Ca^{2+}-binding Domains as Deduced by X-ray Analysis[a] and the Corresponding NOE Contacts Observed in TH2[b]

X-ray	TH2	X-ray	TH2
M138–I149	M135–I146[c]	F102–F154	M135–F151[d]
I113–F154,I149–F154	I146–F151[c]	L98–F154	I131–F151[d]
S141–M157	G138–M154[c]	F105–F154	*e*
F154–M158	F151–M155[c]	F102–F151	*e*
F151–F154	F148–F151[c]	I115–I134	I131–F148[d]
F102–I113	M135–I146[c]	L118–M138	M135–F151[d]
F105–I121	G138–M154[c]	L122–V129	*e*
F105–I113	G138–I146[c]	I113–I149	*f*
I113–L118	I146–F151[c]		

[a] From Figure 7a of Strynadka and James (1989). The residue numbers and sequence of chicken skeletal TnC are used. [b] NOE contacts are indicated by residue pairs rather than by specific proton pairs. [c] Intramonomer contacts. [d] Intermonomer contacts. [e] Corresponding contacts for TH2 not observed in NOESY spectra. [f] The corresponding NOE contacts in NMR spectra would involve Ile146–Ile146 and can not be separated into intra- and intermonomer restraints.

Figure 9 shows the best fit superposition of the C^{α} atoms from Asp128–Glu156 of the restrained energy-minimized mean structure, $\overline{SA}_r$ of TH2 and the corresponding C-terminal fragment from the X-ray structure of chicken skeletal TnC, including helix E–loop III–helix F and helix G–loop IV–helix H. The overall folds are very similar despite an rms difference in the C^{α} positions of 2.5 Å. In addition, the relative orientations of the helices in the dimer are similar to that observed in the X-ray structure of the intact molecule (Strynadka & James, 1989; Herzberg & James, 1988; Satyshur et al., 1988). In the crystal structure, helices G and H are at an angle of ~100° and helices E and H are at an angle of ~130°, while in TH2 the angles between helices G and H and G' and H are ~90° and ~120°, respectively. That small differences occur

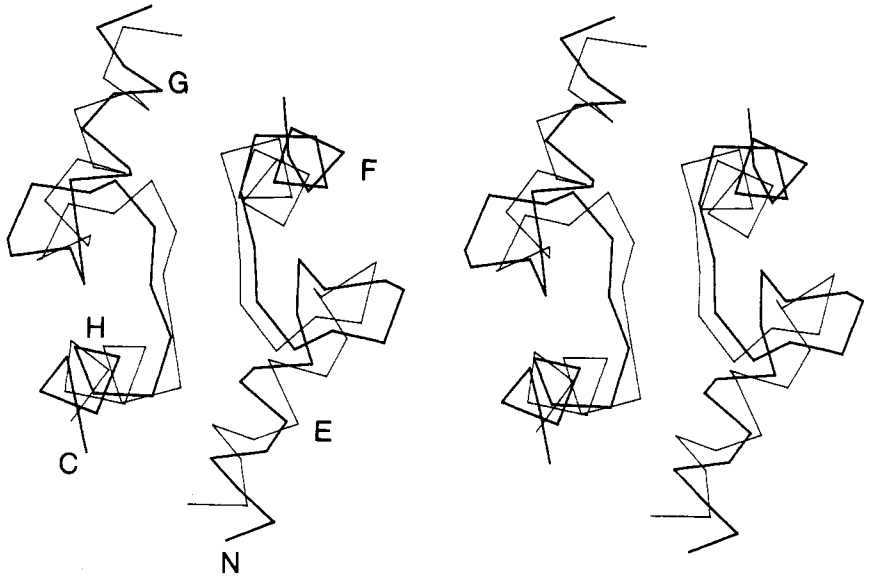

FIGURE 9: Best fit superposition of the C^{α} atoms of Asp128–Glu156 of the restrained energy minimized mean structure of TH2 (thick line) with the corresponding fragments of the X-ray structure of chicken skeletal TnC (Sundaralingam et al., 1985) from residues Glu95 to Arg123 and Glu131 to Glu159. The N- and C-terminal regions of the fragment are indicated by N and C, while helices, E, F, G, and H of chicken skeletal TnC are indicated by the letters E, F, G, and H, respectively. The atomic rms difference between the C^{α} positions in the two structures is 2.5 Å.

between the NMR- and X-ray-based structures is not surprising, considering that in solution two identical fragments containing only site IV dimerize to "mimic" the C-terminal half of TnC. The dimer thus consists of two halves that are equivalent in sequence and that, on the basis of the observation of a single set of resonances in spectra recorded at a number of different temperatures, also appear to be equivalent structurally. This latter feature could be the result of rapid averaging of different conformations or may simply reflect the fact that the monomers form identical stable structures upon dimerization. In contrast, sites III and IV differ both in sequence and structure in the intact molecule. While the differences in sequence are subtle, an rms difference of 0.9 Å in the C^{α} positions in the crystal structure of chicken skeletal TnC between residues Glu95–Arg123 in site III and residues Glu131–Glu159 in site IV is found, and the difference escalates rapidly as more residues closer to the termini of the motifs are included in the comparison. The small differences in sequence between sites III and IV result in the formation of contacts between residues in the intact structure that are not completely duplicated in the dimer formed in solution. For example, the aromatic residues of Phe99 and Phe151 (or homologous residues) pack against one another in the crystal structure of TnC in a manner conserved in all high-resolution structures of Ca^{2+}-binding proteins published to date (Strynadka & James, 1989). The corresponding interaction in the TH2 dimer is one involving Met135 and Phe151, which, as indicated previously, is observed in NOESY spectra. Despite the fact that methionine and phenylalanine have similar sizes and are both hydrophobic, it is possible that the differences between these residues may be significant enough to result in structural changes.

The changes in the sequence between the TH2 dimer and the intact C-terminal domain of TnC, as well as the absence of the polypeptide linker between the two HLH monomers in the fragment dimer, lead to changes in structure and stability. These factors are, in turn, responsible for the decrease in Ca^{2+} affinity in the dimer of 3–4 orders of magnitude (Leavis et al., 1978) relative to the C-terminal sites of the intact protein. Specifically, differences in the interactions between residues in the hydrophobic core described above may partly explain these changes. In this context, it is interesting to note that the molecular evolution of the Ca^{2+}-binding proteins such as TnC and CaM may have proceeded via a tandem duplication of an ancestral gene resulting in domain I being genetically closer to III and II closer to IV (Goodman, 1980). While it is possible for a dimer of domains IV or III (Shaw et al., 1990) to approximate the C-terminal half of TnC, as the present study and that of Shaw et al. (1990) have demonstrated, evolution has provided a better approach involving both sites in which the interactions have been "fine-tuned" over the course of time to result in a highly stable structure.

ACKNOWLEDGMENTS

We are extremely grateful to Drs. G. M. Clore and A. M. Gronenborn for helpful suggestions regarding all aspects of this work and for a critical reading of the manuscript. In addition, discussions with Drs. A. Bax, P. Driscoll, M. Ikura, J. Moult, and M. Nilges are greatly appreciated. We thank Duncan J. McCubbin and Kimio Oikawa for expert technical assistance.

Registry No. Ca, 7440-70-2.

REFERENCES

Arrowsmith, C. H., Pachter, R., Altman, R. B., Iyer, S. B., & Jardetzky, O. (1990) *Biochemistry 29*, 6332–6341.

Babu, Y. S., Bugg, C. E., & Cook, W. J. (1988) *J. Mol. Biol. 203*, 191–204.

Bax, A. (1989) *Methods Enzymol. 176*, 151–158.

Bax, A., Sklenár, V., Clore, G. M., & Gronenborn, A. M. (1987) *J. Am. Chem. Soc. 109*, 7188–7190.

Bodenhausen, G., Vold, R. L., & Vold, R. R. (1980) *J. Magn. Reson. 37*, 93–106.

Braunschweiler, L., & Ernst, R. R. (1983) *J. Magn. Reson. 53*, 521–528.

Brooks, B. R., Bruccoleri, R. E., Olafson, B. D., States, D. J., Swaminathan, S., & Karplus, M. (1983) *J. Comput. Chem. 4*, 187–217.

Brown, S. C., Weber, P. L., & Mueller, L. (1988) *J. Magn. Reson. 77*, 166–169.

Brünger, A. T., (1988) XPLOR Manual, Yale University, New Haven, CT.

Brünger, A. T., Clore, G. M., Gronenborn, A. M., & Karplus, M. (1987) *Protein Eng. 1*, 399–406.
Byers, D. M., & Kay, C. M. (1082) *Biochemistry 21*, 229–233.
Clore, G. M., & Gronenborn, A. M. (1987) *Protein Eng. 1*, 275–288.
Clore, G. M., & Gronenborn, A. M. (1989) *CRC Crit. Rev. Biochem. Mol. Biol. 24*, 479–564.
Clore, G. M., Gronenborn, A. M., Brünger, A. T., & Karplus, M. (1985) *J. Mol. Biol. 186*, 435–455.
Clore, G. M., Brünger, A. T., Karplus, M., & Gronenborn, A. M. (1986) *J. Mol. Biol. 191*, 523–551.
Clore, G. M., Appella, E., Yamada, M., Matsushima, K., & Gronenborn, A. M. (1990) *Biochemistry 29*, 1689–1696.
Clothia, C. (1976) *J. Mol. Biol. 105*, 1–14.
Davis, D. G., & Bax, A. (1985) *J. Am. Chem. Soc. 107*, 2820–2821.
Drakenberg, T., Forsen, S., Thulin, E., & Vogel, H. J. (1987) *J. Biol. Chem. 262*, 672–678.
Driscoll, P. C., Clore, G. M., Beress, L., & Gronenborn, A. M. (1989) *Biochemistry 28*, 2178–2187.
Ebashi, S., & Kodama, A. (1965) *J. Biochem. 58*, 107–108.
Eisenberg, E., & McLachlan, A. D. (1985) *Nature 319*, 199–203.
Goodman, M. (1980) in *Calcium Binding Proteins: Structure and Function* (Siegel, F. L., Carafoli, E., Kretsinger, R. H., MacLennan, D. H., and Wasserman, R. H., Eds.) pp 347–354, Elsevier, North Holland.
Grabarek, Z., Drabikowski, W., Leavis, P. C., Rosenfeld, S. S., & Gergely, J. (1981) *J. Biol. Chem. 256*, 13121–13127.
Grabarek, Z., Leavis, P. C., & Gergely, J. (1986) *J. Biol. Chem. 261*, 608–613.
Havel, T. F. (1986) DISGEO, Quantum Chemistry Program Exchange No. 507, Indiana University, Bloomington, IN.
Havel, T. F., & Wüthrich, K. (1984) *Bull. Math. Biol. 46*, 673–698.
Herzberg, O., & James, M. N. G. (1985) *Nature 313*, 653–659.
Herzberg, O., & James, M. N. G. (1988) *J. Mol. Biol. 203*, 761–779.
Huxley, H. E. (1973) *Cold Spring Harbor Symp. Quant. Biol. 37*, 361–376.
Ikura, M., Minowa, O., Yazawa, M., Yagi, K., & Hikichi, K. (1987) *FEBS Lett. 219*, 17–21.
Janin, J., Miller, S., & Clothia, C. (1988) *J. Mol. Biol. 204*, 155–164.
Jeener, J., Meier, B. H., Bachmann, P., & Ernst, R. R. (1979) *J. Chem. Phys. 71*, 4546–4553.
Jones, A. T. (1978) *J. Appl. Crystallogr. 11*, 268–272.
Kay, C. M., McCubbin, W. D., & Sykes, B. D. (1987) *Biopolymers 26*, 5123–5144.
Kraulis, P. J., Clore, G. M., Nilges, M., Jones, T. A., Pettersson, G., Knowles, J., & Gronenborn, A. M. (1989) *Biochemistry 28*, 7241–7257.
Kretsinger, R. H., & Nockolds, C. E. (1973) *J. Biol. Chem. 248*, 3313–3326.
Leavis, P. C., Rosenfeld, S. S., Gergely, J., Grabarek, Z., & Drabikowski, W. (1978) *J. Biol. Chem. 253*, 5452–5459.
Macura, C., Huang, Y., Suter, D., & Ernst, R. R. (1981) *J. Magn. Reson. 43*, 259–281.
Marion, D., & Wüthrich, K. (1983) *Biochem. Biophys. Res. Commun. 113*, 967–974.
Marion, D., & Bax, A. (1988a) *J. Magn. Reson. 80*, 528–533.
Marion, D., & Bax, A. (1988b) *J. Magn. Reson. 79*, 352–356.
Marsden, B. J., Hodges, R. S., & Sykes, B. D. (1989) *Biochemistry 28*, 8839–8847.
McCubbin, W. D., Oikawa, K., & Kay, C. M. (1986) *FEBS Lett. 195*, 17–22.
Moews, P. C., & Kretsinger, R. H. (1975) *J. Mol. Biol. 91*, 201–228.
Mueller, L. (1987) *J. Magn. Reson. 72*, 191–196.
Neuhaus, D., Wagner, G., Vasak, M., Kagi, J. H. R., & Wüthrich, K. (1985) *Eur. J. Biochem. 151*, 257–273.
Nilges, M., Gronenborn, A. M., & Clore, G. M. (1988a) *FEBS Lett. 229*, 317–324.
Nilges, M., Gronenborn, A. M., Brunger, A. T., & Clore, G. M. (1988b) *Protein Eng. 2*, 27–38.
Nilges, M., Clore, G. M., & Gronenborn, A. M. (1988c) *FEBS Lett. 239*, 129–136.
Nilges, M., Clore, G. M., & Gronenborn, A. M. (1990) *Biopolymers 29*, 813–822.
Plateau, P., & Guéron, M. (1982) *J. Am. Chem. Soc. 104*, 7310–7311.
Redfield, A. G., & Kunz, S. (1975) *J. Magn. Reson. 19*, 250–254.
Satyshur, K. A., Rao, S. T., Pyzalska, D., Drendel, W., Greaser, M., & Sundaralingam, M. (1988) *J. Biol. Chem. 263*, 1628–1647.
Siegel, L. M., & Monty, K. J. (1966) *Biochim. Biophys. Acta 112*, 346–362.
Shaw, G. S., Hodges, R. S., & Sykes, B. D. (1990) *Science 249*, 280–283.
Strynadka, C. J., & James, M. N. G. (1989) *Annu. Rev. Biochem. 58*, 951–998.
Sundaralingam, M., Bergstrom, R., Strasberg, G., Rao, S. T., Roychowdhury, P., Greaser, M., & Wang, B. C. (1985) *Science 227*, 945–948.
Swain, A. (1988) Ph.D. Thesis, University of South Carolina.
Szebenyi, D. M. E., & Moffat, K. (1986) *J. Biol. Chem. 261*, 8761–8777.
Tao, T., Gowell, E., Strasberg, G. M., Gergely, J., & Leavis, P. C. (1989) *Biochemistry 28*, 5902–5908.
Weiss, M. A. (1990) *J. Magn. Reson. 86*, 626–632.
Wüthrich, K. (1986) *NMR of Proteins and Nucleic Acids*, Wiley, New York.
Wüthrich, K. (1989) *Acc. Chem. Res. 22*, 36–44.